Nanoscale

Percolative phase transition in few-layered $MoSe_2$ Field-effect transistors using Co and Cr contacts

Journal:	*Nanoscale*
Manuscript ID	NR-ART-09-2024-003986.R1
Article Type:	Paper
Date Submitted by the Author:	03-Dec-2024

Complete List of Authors:	Padhan, Roshan; Jackson State University, Department of Chemistry, Physics and Atmospheric Science Garcia, Carlos; National High Magnetic Field Laboratory Kadam, Sujit; Jackson State University, Department of Chemistry, Physics and Atmospheric Science Wali, Akshay; Jackson State University, Department of Chemistry, Physics and Atmospheric Science; Argonne National Laboratory McGill, Stephen; National High Magnetic Field Laboratory Pradhan, Nihar; Jackson State University, Department of Chemistry, Physics and Atmospheric Science Divan, Ralu; Argonne National Laboratory, Center for Nanoscale Materials Sumant, Anirudha; Argonne National Laboratory, Centre for NanoMaterials Rosenmann, Daniel; Argonne National Laboratory Miller, Suzanne; Argonne National Laboratory, Center for Nanoscale Materials

Percolative phase transition in few-layered $MoSe_2$ Field-effect transistors using Co and Cr contacts

Roshan Padhan,[1] Carlos Garcia,[2] Ralu Divan,[3] Anirudha V. Sumant,[3] Daniel Rosenmann,[3] Sujit A. Kadam,[1] Akshay Wali[1,3], Suzanne Miller,[3] Stephen McGill,[2*] Nihar R. Pradhan[1*]

[1]Layered Materials and Device Physics Laboratory, Department of Chemistry, Physics and Atmospheric Science, Jackson State University, Jackson, MS 39217, USA.

[2]National High Magnetic Field Laboratory, 1800 E. Paul Dirac Dr., Tallahassee, FL 32310, USA.

[3]Center for Nanoscale Materials, Argonne National Laboratory, 9700 S-Cass Avenue, Lemont, IL-60439, USA

[*]Email: nihar.r.pradhan@jsums.edu , mcgill@magnet.fsu.edu

Abstract

The metal-to-insulator phase transition (MIT) in two-dimensional (2D) materials under the influence of a gating electric field has revealed interesting electronic behavior and the need for a deeper fundamental understanding of electron transport processes, while attracting great interest on the development of next-generation electronic and optoelectronic devices. Although the mechanism of the MIT in 2D semiconductors is a topic under debate in condensed matter physics, our work demonstrate the tunable percolative phase transition in few-layered $MoSe_2$ field-effect transistors (FET)using different metallic contact materials. Here, we attempted to understand the MIT through temperature-dependent electronic transport measurements by tuning the carrier density in $MoSe_2$ channel under the influence of applied gate voltage. In particular, we have examined this phenomenon using the conventional chromium (Cr) and ferromagnetic cobalt (Co) as two metal contacts. For both Cr and Co, our devices demonstrated an *n*-type behavior with a room-temperature field-effect mobility of 16 $cm^2V^{-1}s^{-1}$ for the device with Cr contacts and 92 $cm^2V^{-1}s^{-1}$, respectively. At low temperature measurements of 50K, the mobilities increased significantly to 65 $cm^2V^{-1}s^{-1}$ for Cr and 394 $cm^2V^{-1}s^{-1}$ for the device with Co contacts. By fitting our experimental data to the percolative phase transition theory, the temperature-dependent conductivity data shows a transition from an insulating-to-metallic behavior at a bias of ~28 V for Cr contacts and ~20 V for Co contacts. This cross-over of the conductivity can be attributed to increasing carrier density as a function of gate bias in the temperature-dependent transfer characteristics. By extracting the critical exponents, we find that the transport behavior in device with Co contacts aligns closely with the 2D percolation theory. In contrast, the devices with Cr-contacted deviate significantly from the 2D limit at low temperatures.

I. Introduction

The rapid advancement of technology has intensified the demand for more efficient and high-performance devices.[1] With the growing use of smartphones, laptops, and data centers, there is an urgent need to address the increasing energy consumption and heat generation associated with these technologies.[2] There is an ongoing quest to explore quantum materials with tunable electronic properties for data storage and processing applications. Studying the metal-to-insulator transition (MIT) is particularly significant among various research avenues within two-dimensional (2D) systems. [3–6] MIT materials uniquely offer the ability to dynamically and reversibly switch between metallic and insulating states, reducing power consumption and significantly lowering heat generation. [3,6,7] This capability is crucial for the next generation of computing, communication, and storage technologies, as it enables faster and more reliable switching mechanisms while enhancing overall device efficiency.[3,8] Recent advancements in 2D transistors, such as sub-1 nm MoS_2 FETs, underscore the transformative potential of 2D materials in addressing scaling limitations and mitigating heat dissipation, further emphasizing the importance of studying MIT phenomena in these systems.[9] The theoretical foundation for understanding MITs in reduced dimensions was laid by the scaling theory of localization proposed by Abrahams *et al.*[10] which demonstrated that true metallic behavior is absent in two-dimensional disordered systems. Their work revealed how electronic conductance transitions from logarithmic to exponential decay with increasing disorder or reduced system size, providing critical insights into transport phenomena at the nanoscale.

Among quantum materials, 2D transition-metal dichalcogenides (TMDCs) are ideal for studying the MIT due to their precise layer-dependent properties, high surface-to-volume ratio, and unique quantum confinement effects.[11–13] Their sensitivity to external stimuli allows for more controllable MIT behavior. At the same time, their flexibility and ease of integration into various device architectures enhance their utility in exploring and utilizing MIT phenomena.[12,13] Additionally, strong electron correlation effects in these materials make them particularly suited for examining the transition between metallic and insulating states. Among various 2D materials, $MoSe_2$ is particularly interesting due to its pronounced layer-dependent electronic properties, which shift from a direct to an indirect bandgap with changes in thickness.[14–16] Its high stability, tunable properties, and compatibility with other 2D materials make it an excellent candidate for studying the MIT.[13–15,17] Further, $MoSe_2$ demonstrates

superior FET device performance due to its high carrier mobility, excellent electrostatic control, and scalable fabrication, all of which enhance its ability to modulate current flow effectively in response to an applied electric field. [6,18–20]

This research extends our previous investigation of the MIT in few-layer $MoSe_2$ FETs at low temperatures, demonstrating tunable temperature scaling of the MIT, by using both traditional non-magnetic metallic and ferromagnetic contacts.[15] We explored the temperature-dependent transport properties of the 2D $MoSe_2$ devices using Cr and Co contacts, which showed n-type behavior. The temperature-dependent conductivity data revealed an insulator-to-metal transition as a function of increasing carrier density, analyzed through theoretical fits to the Fermi-Liquid T^2-dependent relation. The temperature-dependent 4-terminal conductivities were analyzed with temperature-dependent percolation theory and showed close agreement to a percolation-driven MIT throughout the studied temperature range for Co contacts, while the Cr contacted sample deviated from the predictions of 2D percolation theory. The extracted critical exponents indicated that devices with Co contacts closely followed 2D percolation theory across the temperature range, whereas devices with Cr contacts deviated from the 2D limit at low temperatures. The temperature-dependent data were also analyzed to understand the transport behavior through Schottky barrier height (SBH). This work revealed the large difference in SBH between Cr- and Co-contacted $MoSe_2$ devices that may also tune the MIT properties.

II. Results and Discussion

The $MoSe_2$ crystals were grown using the chemical vapor transport method and characterized before exploring temperature-dependent transport studies.[15] Raman spectroscopy was employed to verify the quality of the crystal. Thin layers of flakes were mechanically exfoliated using blue tape and transferred onto a clean 285 nm thick SiO_2 layer deposited on the highly p-doped silicon substrate. The contacts were fabricated using Laser Writer-based optical lithographic techniques, followed by e-beam evaporation (Lesker PVD 250 at a base pressure of 10^{-8} Torr) of Au (80 nm)/Cr (5 nm) for Au/Cr contacts and Au (80 nm)/Co (10nm) for Au/Co contacts. Several devices were also fabricated using Temescal e-beam evaporator in clean room environment. The thickness of the $MoSe_2$ layer was 7 -15 nm as measured by atomic force microscopy. Figure 1 (a) shows the optical micrograph image of the 7 nm thick $MoSe_2$ FET devices with contacts of 5 nm Cr and 80 nm Au. Figure 1(b) shows a 7 nm thick $MoSe_2$ device with 10 nm Co and 80 nm Au fabricated on the 285 nm SiO_2 substrate

deposited on highly p-doped Si. The thickness of the devices were measured using Veeco Dimension Atomic Force Microscopy (AFM). The AFM topography and height measurements are shown in the supporting information figure S1. The devices were covered with a thin layer of Cytop polymer to protect them from direct contact with the ambient atmosphere. Transport measurements shown in the Figure 1 were carried out using 2-terminal method and all temperature dependent transport measurements were performed using the 4-terminal method shown in the Figure 2- 5 to eliminate the associated resistance of the contacts. We measured the drain-source current (I_{ds}) as a function of drain-source voltage (V_{ds}) using two terminal and shown in Fig. 1 (c-d) for Cr cntact $MoSe_2$ (Cr-$MoSe_2$) and Co contact $MoSe_2$ (C-$MoSe_2$) FETs at different applied gate voltages (V_{bg}). We observed linear *I-V* curve on both Cr- and Co-contacted devices despited they were Schottky contact due to the thermionic emission process at room temperature. Figure (e-f) shows the transistor characteristic I_{ds} as a function of applied gate voltage V_{bg} for Cr-$MoSe_2$ and Co-$MoSe_2$ respectively.

The drain current shows higher in Co-$MoSe_2$ device compared to the Cr-$MoSe_2$ on both the devices with same thickness of $MoSe_2$, which indicate the Co contact could be better than the Cr contact on $MoSe_2$. The extracted field effect mobilities using Si-MOSFET formula for 2-terminal device $\mu_{FE} = \frac{L}{WC_{ox}V_{ds}} \times \left(\frac{dI_{ds}}{dV_{bg}}\right)$, yields the mobility values of 6.5 cm^2/Vs and 15.2 cm^2/Vs for Cr-$MoSe_2$ and Co-$MoSe_2$ respectively. The parameters L is the channel length between two current contacts where V_{ds} was applied and current was measuredon the same outer (current) contacts. C_{ox} = 11:505 × 10^{-9} F/cm^2 is the capacitance/unit area between the gate and the channel for a 285 nm layer of SiO_2 $C_{ox} = {\varepsilon_o\varepsilon_r}/{d}$, ε_r =3.9 for SiO_2 and d = 300 nm. We also measured the four-terminal transport measurements for these devices shown in the supporting Fig. S2. Fig S2 (a-b) presented the I_{ds} vs V_{bg} of the Cr-$MoSe_2$ and $CoMoSe_2$ devices. The four-terminal mobility values are extracted using the MOSFET relation $\mu_{FE} = \frac{l}{WC_{ox}}\left(\frac{d(I_{ds}-I_o)/V_{12}}{dV_{bg}}\right)$, where l is the channel length of the devices between two voltage contacts (inner contacts in 4-terminal measurements) 9.5 μm for the Cr contact device & 8 μm for the Co contact device), W is the width of the channel of the devices and the values are 5.4 μm for Cr & 4.78 μm for Co contacts. C_{ox} is the gate capacitance as stated before and I_o is the current in the subthreshold regime. V_{12} is the voltage voltage sense between two voltage conatcts (inner contacts) in 4-terminal measurements. The value of $\left(\frac{d(I_{ds}-I_o)/V_{12}}{dV_{bg}}\right)$, was extracted from

the slope of the I_{ds} curve in the linear region. In both cases, μ_{FE} increased with decreasing temperature.[6,21–25] We found the field effect mobility at room temperature of these devices increases to 16 cm^2/Vs and 45.5 cm^2/Vs for Cr-$MoSe_2$ and Co-$MoSe_2$ FETs in 4-terminal measurements.

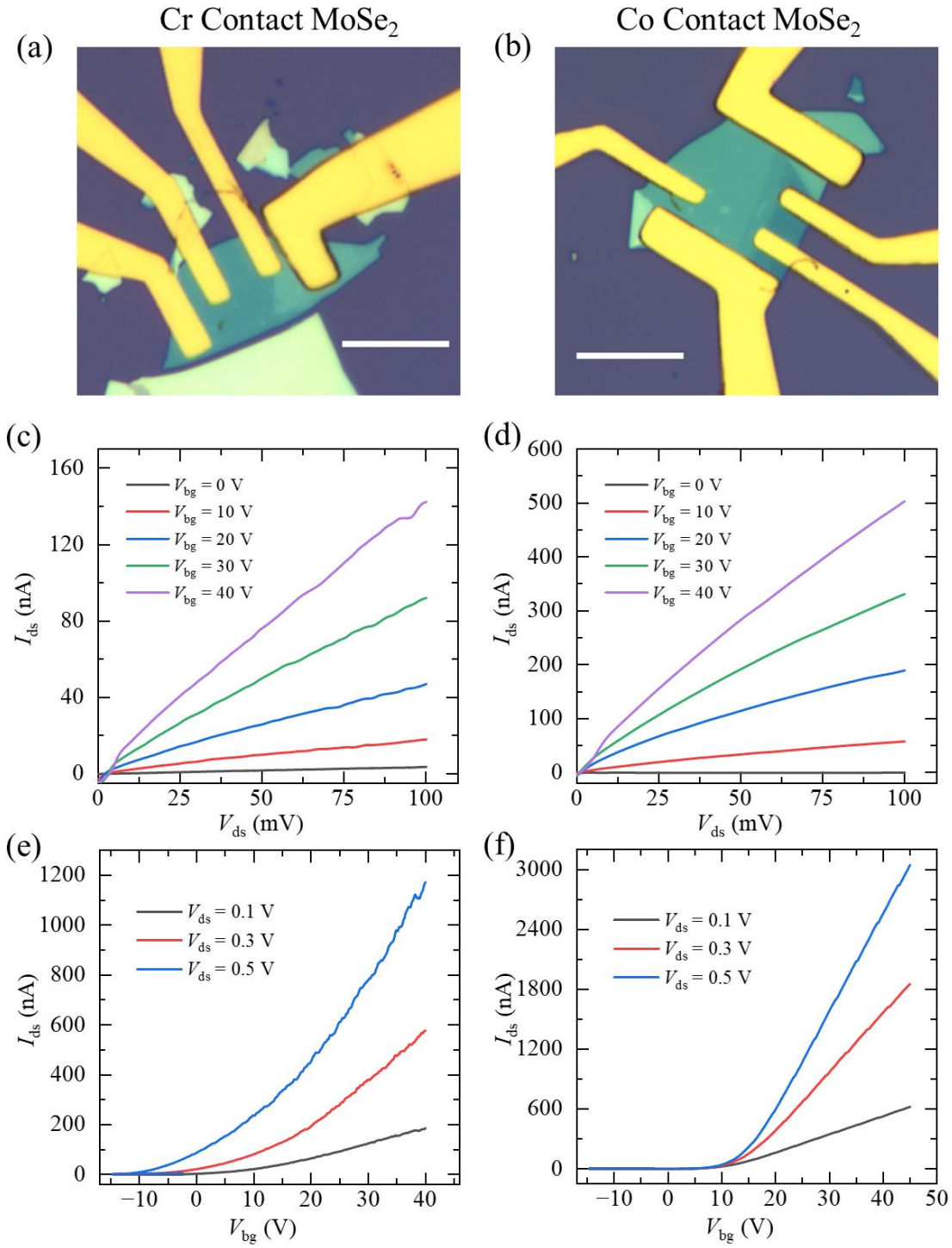

Figure. 1 Room Temperature FET Characterizations: (a-b) Optical micrograph of $MoSe_2$ Devices with Co/Au contact and Cr/Au contact (Scale bar: 10 μm), (c-d) Basic Output Characteristics of FET at different back-gate voltages (V_{bg}) for both Co and Cr contact $MoSe_2$

FETs measured at room temperature, (e-f) Transfer Characteristics of FETs at different Source-drain voltages (V_{ds}).

.Figure S2 (c-d) represent the comparision plots of 2- and 4-terminal measurements of transport curves from where we extracted the contact resistance of the device using the relation $R_c = \frac{1}{2}\left(\frac{V_{ds}}{I_{2T}} - \frac{V_{ds}}{I_{4T}}\right)$ where I_{2T} and I_{4T} are the drain current measured from the 2 and 4-terminal configurations respectively. The contact resistance shown in the Fig. S2 (e-f) suggested higher value in Cr-$MoSe_2$ compared to the Co-$MoSe_2$ FET. The R_c values for Cr-$MoSe_2$ and Co-$MoSe_2$ devices are 3 MΩ, 2.7 MΩ (at V_g = 15V), 1.6 MΩ, 1.2 MΩ (at V_g = 20V) and 600 KΩ, 200 KΩ (at V_g = 35V). This could explain why Co-$MoSe_2$ device performs better than Cr-$MoSe_2$ FET. Our aim was to explore the temperature-dependent transport behavior of the FET based on these two different metal contacts and how the conductivities could be tuned as a function of applied gate voltage (i.e., charge carrier density). The conductivities revealed the intrinsic behavior of the $MoSe_2$ when analyzed with temperature-dependent scaling. We measure another sets of devices for temperature dependent study describe below. Figures 2(a) and 2(b) display the four-terminal drain-source current, I_{ds}, as a function of back gate voltage, V_{bg}, at several different temperatures under a constant drain-source voltage of V_{ds} = 500 mV for the devices with Cr and Co contacts, respectively. The device showed n-type FET behavior, similar to earlier reports on $MoSe_2$-based FET devices.[15,26] The threshold voltage was ~20V for both devices, and at V_{bg} = 0 V, a charge carrier density of n ~1.59×10^{12}/cm^2 was induced in the $MoSe_2$ channel. The semi-logarithmic scaled I_{ds} as a function of V_{bg} are presented in Figs. 2(c & d) for both Cr- and Co- contacted devices. The observed ON/OFF current ratio of ~10^5 showed the comparable performance of the previously reported multilayered TMDC-based devices.[15,23,27,28] Figures 2(e & f) display the extracted field-effect mobilities as a function of temperature for Cr- and Co- contacted devices. The field-effect mobilities were extracted from the semiconducting MOSFET relation as explied before where l is the channel length of the devices between two voltage contacts (9.5 μm for the Cr contact device & 8 μm for the Co contact devices), W is the width of the fabricated devices (5.4 μm for Cr & 4.78 μm for Co contact devices). As shown in Figure 2(e), for the Cr-contacted device, μ_{FE} was determined to be 16 cm^{2}V^{-1}S^{-1} at 263 K and 65 cm^{2}V^{-1}S^{-1} when cooled to 61 K. In contrast, the field-effect mobility for the Co-contacted FET (Figure 2(f)) was 92 cm^{2}V^{-1}S^{-1} at 217 K and increased to 394.8 cm^{2}V^{-1}S^{-1} when cooled to 1.7 K. Such a difference in mobility for the Co-contacted $MoSe_2$ device demonstrates the

significance of using a suitable contact with a high charge injection capacity. Furthermore, cobalt is ferromagnetic, and spin current injection could be another factor that could potentially lead to a reduction in scattering mechanisms through spin-orbit coupling, thereby indirectly enhancing mobility by mitigating certain types of electron scattering events in the Co-$MoSe_2$ device. The mobility obtained is considerably higher than those previously reported $MoSe_2$-based field-effect transistors with traditional metal contacts.[29–31] Furthermore, for both types of contacts, these devices showed strongly *T*-dependent mobilities, indicating phonon and impurity scattering. At lower temperatures, the phonon scattering of the sample was minimized, resulting in electron mobility being limited by the scattering by impurities and crystal defects. In general, electron-phonon (e-ph) scattering plays a key role in carrier mobility near room temperature.[32,33] Longitudinal optical (LO) phonon scattering limits the intrinsic mobility of most transition metal dichalcogenides, while for MoS_2 and WS_2, the mobility is limited by longitudinal acoustic (LA) phonon scattering.[32]

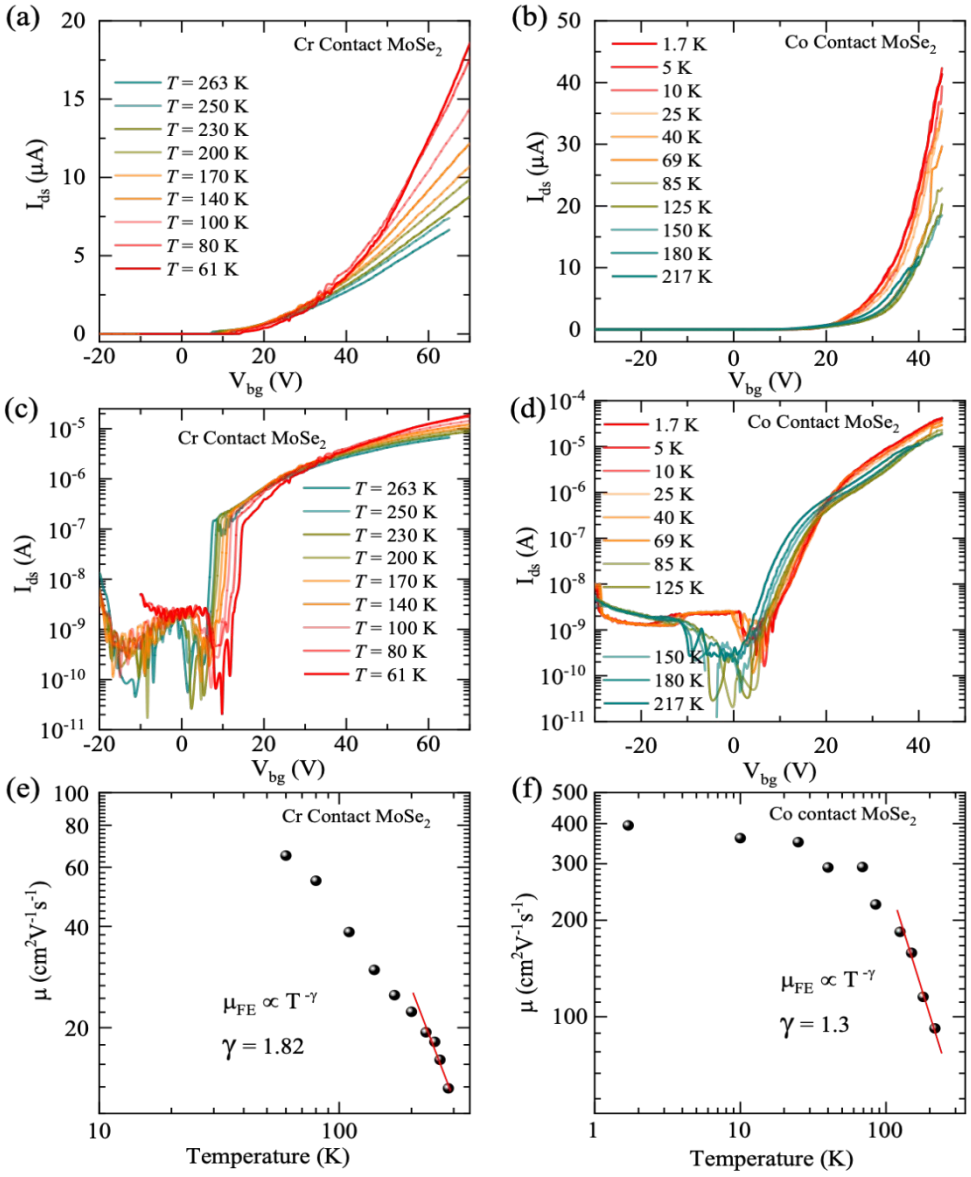

Figure. 2 Temperature dependent Electrical Transport Measurement: (a) and (b) Transfer characteristics of $MoSe_2$ FET at different temperatures for Cr contacts and Co contacts, respectively, measured at V_{ds} = 500mV, (c) and (d) Transfer Characteristics of $MoSe_2$ FET at different temperatures for Cr contacts and Co contacts in semi-logarithmic scale, (e) and (f) display the temperature dependent field-effect mobility of the $MoSe_2$ devices for Cr and Co contacts, respectively. (The red line indicates the power law fitting for the phonon-limited mobility).

Following the phonon scattering theory, we fitted the *T*-dependent mobility to the power law, i.e., $\mu_{FE} \propto T^{-\gamma}$, where γ = phonon scattering exponent. The γ value for the Cr-contacted $MoSe_2$ FET was 1.82, whereas it was 1.3 for the Co-contacted $MoSe_2$ FET. The smaller γ for Co-contacted $MoSe_2$ is associated with a comparatively lower phonon scattering than the Cr-contacted device. Below 70 K, the phonon scattering is almost minimized; however, scattering due to impurity and defects states, carrier localization, and the Schottky barrier

leads to a saturation in the *T*-dependent mobility. The Co-contacted device showed the highest mobility, ~400 $cm^2V^{-1}s^{-1}$ between 10 and 2K. Similar T-dependent mobility was reported on $MoSe_2$ FETs fabricated on a SiO_2/Si substrate.[15]

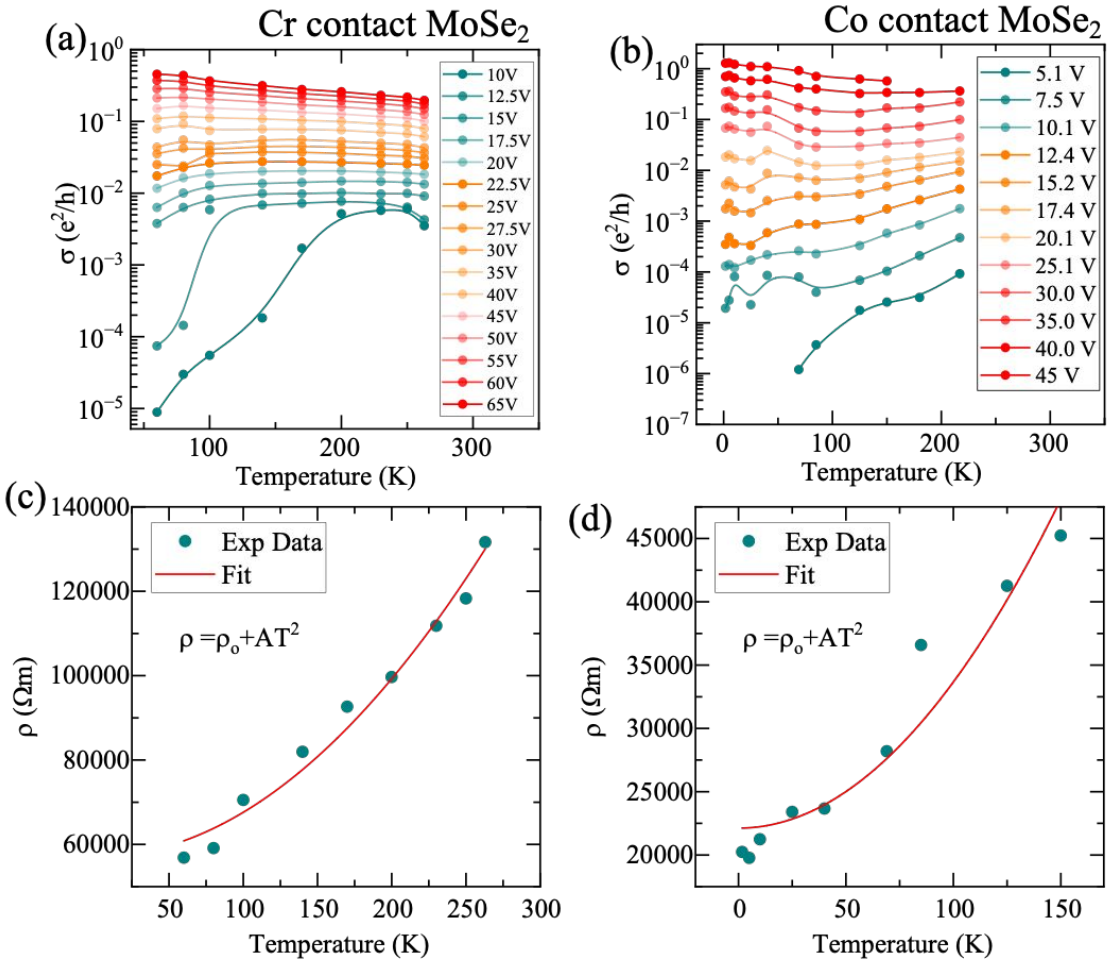

Figure. 3 Temperature-dependent conductivity variations: (a-b) T-dependent conductivity at different back-gate voltage for Cr contacts and Co contacts, (c-d) Fermi-liquid model fitting of resistivity at a back-gate voltage of 20V, for Cr contacts and Co contacts.

Figure 3 displays a deeper analysis of the temperature-dependent conductivities of the Cr- and Co-contacted $MoSe_2$ devices. The quantized conductivity (σ) was calculated from the temperature dependent I_{ds} vs V_{bg} graph using the relation, $\sigma = \frac{WI_{ds}}{lV_{ds}} \times \frac{e^2}{h}$, where e is the charge of the electron and h is Planck's constant. The 4-terminal conductivity as a function of temperature at several applied back gate voltages is depicted in Fig. 3(a) for the Cr-contacted $MoSe_2$ FET. This device showed typically semiconducting behavior below $V_g = 27.5$ V, i.e., σ decreased with decreasing temperature. Conversely, above the applied gate voltage of 27.5 V, the device showed metallic behavior, i.e., σ increased with decreasing temperature. This

infers that, upon injecting a high carrier density, the metallic phase emerged from the insulating phase at low temperature. We also performed the similar *T*-dependent conductivity analysis for the Co-contacted device at different gate voltages (5.1 V to 45 V) as depicted in Figure 3(b). In this case, the transition from metallic to insulating behavior was observed at a comparatively lower back gate voltage of 20.1 V. To elucidate the nature of the phase transition, we renormalized the *T*-dependent conductivity plot by a critical conductivity (σ_c), acquired from the transition point (V_{bg} = 27.5 V for Cr contacts and V_{bg} = 20.1 V for Co contacts) as shown in supplementary material and then scale with the temperature parameter To (Supporting Fig. S3). However the temperature scaling failed similar to the previously reported Cr contact. [15] However, our temperature dependent scaling of the conductivity and critical exponent more closely matched with the percolation type of phase transition as discussed below. According to the Fermi-liquid model of conductors, the resistivity ($\rho = \sigma^{-1}$) is related to temperature through the relation $\rho = \rho_0 + AT^2$, where ρ_0 is the resistivity at 0 K. To verify the metallic behavior at higher gate voltages, we evaluated the resistivity of the channel as a function of temperature. Figure 3(c) shows the resistivity of Cr-contacted $MoSe_2$ at an applied backgate voltage, V_{bg} = 45 V, and figure 3(d) shows the resistivity of the Co-contacted device at V_{bg} = 65 V. In both cases, the data fits the fermi-liquid equation well, as indicated by the red-line of the plot. A similar metallic conductivity was observed in ReS_2 where the resistivity was fitted with the Fermi-liquid T^2 dependent equation throughout the temperature range at higher carrier density or applied gate voltage.[34] This theoretical fitting shows the benchmark of metallic behavior of the $MoSe_2$.

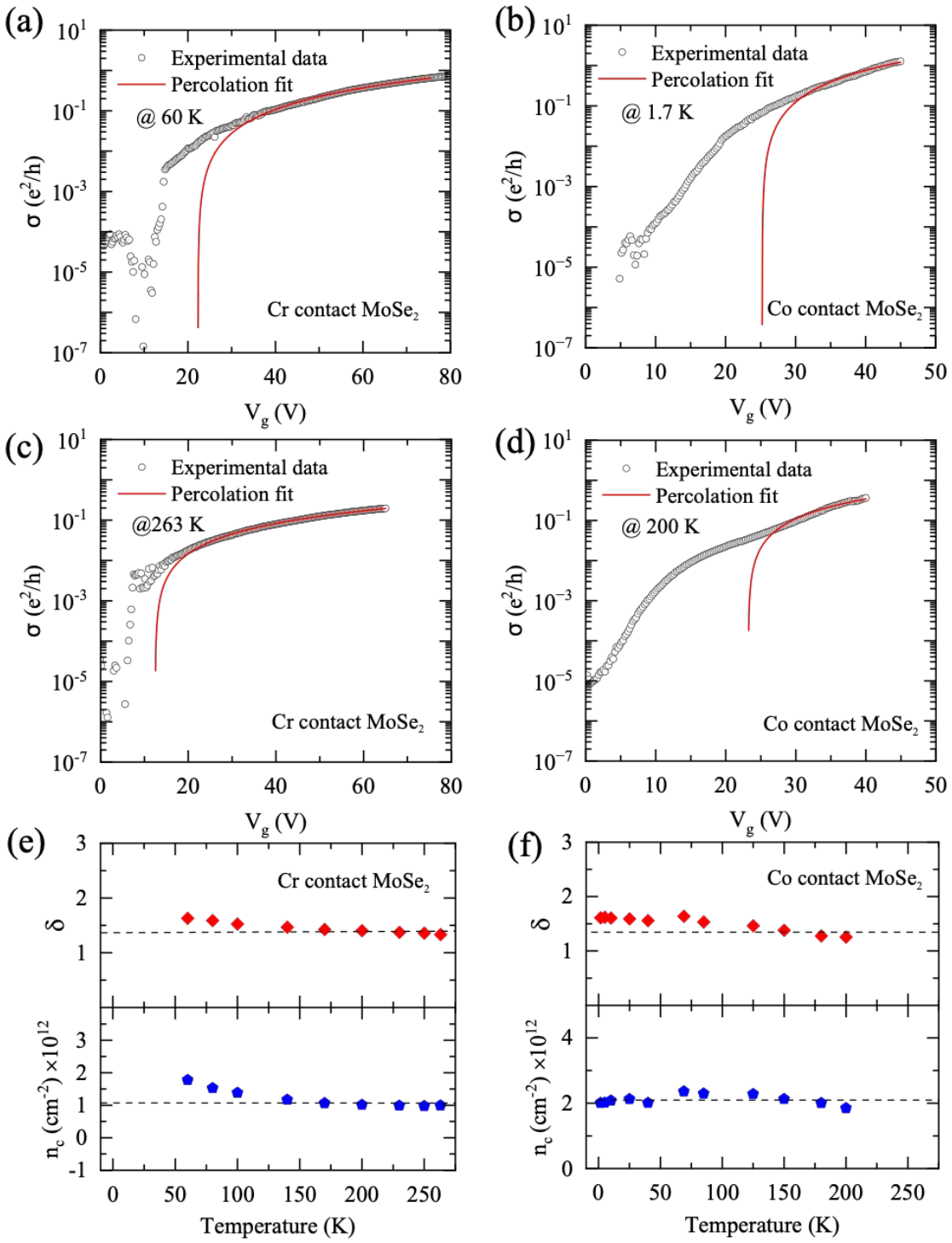

Figure. 4 Percolation type phase transition model: The percolation fitting in the conductivity variation data w.r.t back-gate voltage at various temperatures (a & c) for Cr-contacted and (b & d) for Co-contacted $MoSe_2$ devices, (e & f) display the extracted values of the critical exponent and critical carrier density for Cr contacts and Co contacts in the above fitting at different temperatures.

We analyzed the temperature-dependent conductivities with the percolation model, and the data are presented in Fig. 4. The temperature-scaled percolation model formulates the relation between conductivity (σ) and the carrier density (n) as $\sigma = A(n - n_c)^{\delta}$, where, n_c is the critical carrier density beyond which the carriers can form a percolating path in the random network of charged carriers between the source and the drain.[22,35] From the theoretical predictions, $\delta = 1.33$ for 2D percolation.[15,19,22,36] The density of charge carriers induced at the interface can be controlled by applying the back gate voltage. The induced carriers can be obtained from the relation $n = C_{ox} \times V_{bg}/e$, hence the percolation prediction for the conductivity can be written in terms of V_{bg} as $\sigma = (A \times C_{ox}/e)(V_{bg} - V_c)^{\delta}$, where V_c is the critical back gate voltage. We fitted all the temperature-dependent curves with the percolation fits, and two of those fits are shown in Figs. 4 (a & c) for the Cr-contacted $MoSe_2$ device. Similarly, the percolation fits for the Co-contacted $MoSe_2$ device are shown in Figs. 4 (b & d). More temperature dependent percolation fits are shown in the Supporting information Figure S4 and S5. We extracted the critical exponent δ and V_c from where critical carrier density n_c was calculated. The δ and the n_c was plotted as a function of temperature and presented in Figs. 4 (e) and 4 (f), respectively, for Cr- and Co-contacted $MoSe_2$ devices. For Cr contacts, the critical exponent almost lies between 1.33 to 1.4, which is the theoretical predicted value of 2D percolation phase transition, δ = 1.33. The δ value deviated from the theoretical prediction when the device was cooled below 100 K reaching 1.63 at 61 K. For Cr-contacts, the critical carrier density (n_c) showed a slight increase with decreasing temperature while the Co-contacted device showed almost temperature independent carrier density. Due to the low contact resistance (R_c) in the Co device, the current (or conductivity) values showed saturation at such applied gate voltages compared to the high contact resistance in the Cr-contacted device as we decreased the temperature. The I_{ds} vs V_g data in Figure 2 (a) and (b) or (c) and (d) shows that the conductivity values in the Co-contacted device were nearly four times higher than in the Cr-contacted device. Thus, the carrier density as a function of temperature show still increasing in Cr-contact compared to the Co-contact device. This behavior suggests that Co contacts provide a more efficient carrier injection mechanism, even at low temperatures, leading to the constant n_c values. These differences reflect the distinct interaction of Cr and Co with $MoSe_2$, likely arising from variations in their work functions, interface chemistry, and surface roughness. Previously, Pradhan et. al.,[15] reported that the value becomes ~2 at 5 K.[2] However, by changing this contact to Co, we have achieved a consistent value near the theoretical predicted value even at

low temperature down to 1.7 K. The constant term, A, depends upon factors like: contact resistance (R_c), surface roughness, and the measurement method (i.e., 4-wire/2-wire measurement). Hence, we also found different values of A in the fabricated $MoSe_2$ devices by changing the type of contacts. From the percolation fitting the value of A was found to be 0.01 for the Cr contacts and 0.001 for the Co contacts.

The obtained critical carrier densities for both Cr- and Co-contacted $MoSe_2$ as a function of temperature are displayed in Figs. 4 (e) & (f). For Cr contacts we obtained the average critical carrier density n_c ~1 × 10^{12} cm^{-2} (dashed line in Fig 4e). In contrast, a higher n_c of ~2 × 10^{12} cm^{-2} was achieved in the Co-contacted $MoSe_2$ FET.

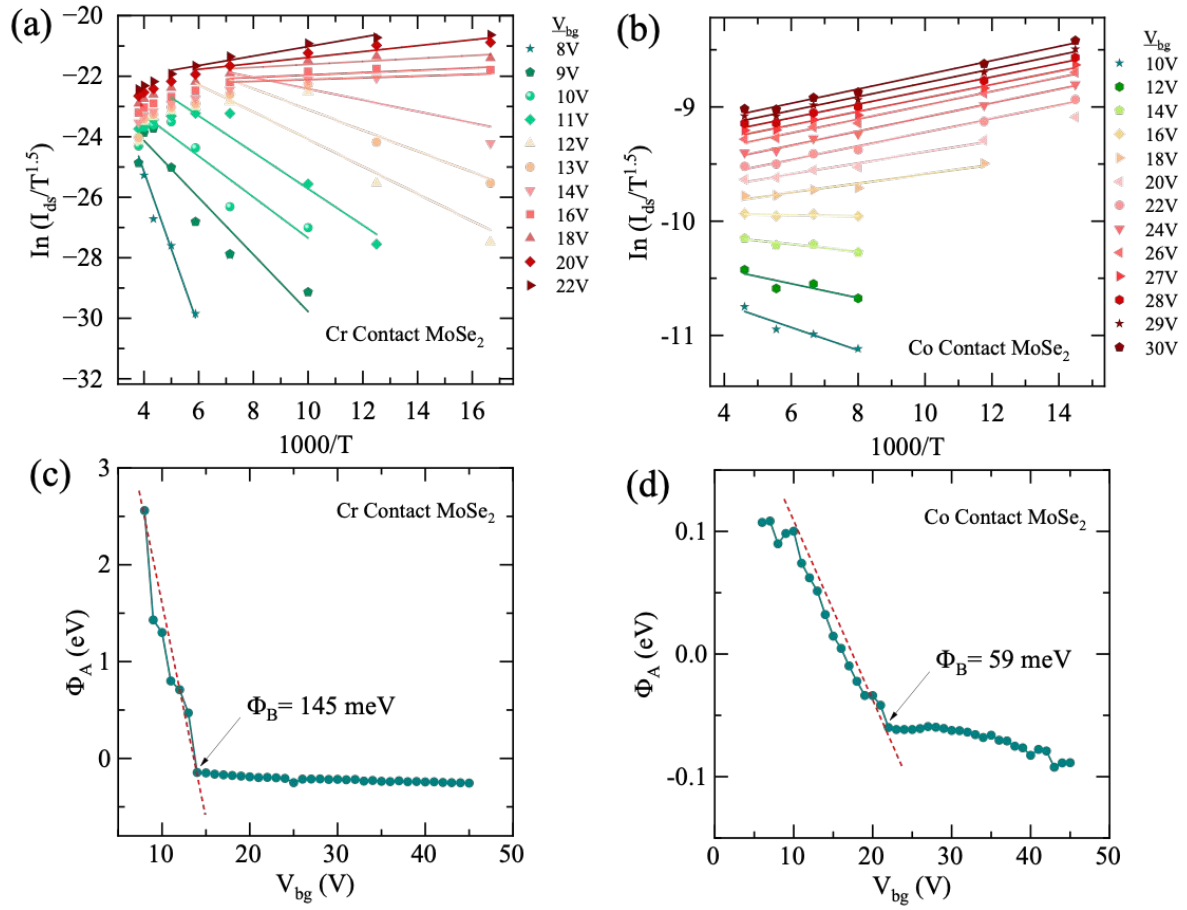

Figure. 5 Schottky Barrier Height calculation: (a-b) Arrhenius Plot for Cr contacts and Co contacts at different back-gate voltages, (c-d) Activation energy as a function of back-gate voltage for both contact types (Schottky Barrier height was extracted from the curve).

So far, from the above discussion of our conductivity analysis, the Co-contacted $MoSe_2$ device showed a stable 2D percolative phase transition and much higher charge carrier

mobility than the Cr-contacted device. To further examine the stability of the Co/$MoSe_2$ interface and analyze the carrier injection from metal to semiconductor, we extracted the Schottky barrier height (SBH) for both types of contacts. The SBH was extracted from the temperature-dependent transfer characteristics of a 2D FET using the following Arrhenius equation for thermionic emission in a 2D system:[6,27,37,38]

$$ln(I_{ds}/T^{3/2}) = \ln A + \ln A_{2d} - \frac{\Phi_A}{K_B}\left(\frac{1}{T}\right)$$

Where, A_{2d} is Richardson's constant in a 2D system, A is the area of the contact, K_B is the Boltzmann constant, and Φ_A is the activation energy. This equation is the linear form of the well-known Arrhenius plot. The slope of the Arrhenius plot gives the activation energy required to drive the carrier through the energy barrier. The Arrhenius plots for the Cr and Co contacts at different gate voltages are displayed in Figures 5(a-b). As suggested by the equation, the SBH can be extracted from the slope of the Arrhenius plot. The activation energies at different back-gate voltages are plotted in Figures 5 (c-d) for both Cr- and Co-contacted $MoSe_2$. In these plots, the Schottky barrier height is the activation energy at the flat band condition of the band diagram, seen as the point at which the activation energy ceases to decrease linearly with gate voltage.[29] This analysis technique has been used to measure the SBH of 100's of meV [31,38–40] in transition metal dichalcogenide-based devices such as MoS_2, WSe_2. Using this same technique, we extracted an SBH of 145 meV for the Cr-contacted $MoSe_2$ FET, whereas we obtained a much smaller SBH of 59 meV for the Co-contact $MoSe_2$ FET. This SBH is very similar to the value measured by Cui et al. using Co contacts.[30] on a MoS_2 device thrpugh a h-BN tunnel barrier. The SBH could be further reduced using spacer materials like h-BN, which helps modify Co's work function and acts as a tunneling barrier for spin current injection to provide higher tunneling current from channel to drain contact. The Ferromagnetic (FM) Co contacts likely plays a significant role in enhancing tunneling and spin-polarized current injection, which may influences the Metal-Insulator Transition (MIT). However, the nature of direct spin current injection from 2D semiconductor to FM contacts is still elusive. Several reserch groups [29,30] realized the spin current injection from 2D semiconductor to FM metal contact through thin layer of TiO_2 or h-BN tunnel barrier, which modify the work function of FM metal contact on 2D semiconductor to reduce the SBH. In our device Co was directly contacted with $MoSe_2$ layer without any tunnel barrier layer. The FM Co contact on $MoSe_2$ results metal-induced gap states (MIGS) which is not only influenced work function like Cr contact (non-magnetic contacts), but also by the additional

interaction with the magnetic moments at the interface of the ferromagnetic metal and 2D semiconductor. This may influence the change in electronic structure at the interface, potentially affecting the spin polarization and transport properties of the Co contact $MoSe_2$ device. Specifically, the magnetic interaction of Co contact can further modify the energy levels of $MoSe_2$ bandgap, creating unique MIGS characteristics compared to a non-magnetic Cr contact. This could be the result of such high conductivity in our Co contact $MoSe_2$ devices compared to the Cr contact devices. These values indicate the FM Co contact is better than the Cr contact on our $MoSe_2$ devices. Similarly, other magnetic contacts such as Fe and Ni could provide comparable advantages due to their magnetic properties and work function values, which may yield low SBH. All these FM contacts could also be effective for spin current injection when contacted with the suitable tunnel barrier layer between FM contact and 2D semiconductor. Furthermore, hybridization between the metal and 2D semiconductor interface may influence charge transfer and tunneling mechanisms. Magnetic metals like Co enhance interface resonances and tune the density of states, leading to improved carrier transport.[41] Furthermore, In contrast, nonmagnetic Cr contacts experience weaker hybridization and stronger Fermi-level pinning, contributing to the higher SBH.[42] This low SBH value is one of the key parameters for achieving high mobility on the Co-contacted device at low temperatures. A similarly low SBH was also reported using magnetic Permalloy[37,43] and Co-contacted MoS_2 FETs.[31] In addition to the work function of the metal contacts, interface states are more important for tuning the SBH at the 2D semiconductor and metal junction. In contrast to the effect of strong Fermi level pinning using different metal contacts, where the band bending dominates the charge transfer mechanism, the interface resonances can dominate the size of the effective barrier by enhancing the tunneling current through the different metal contacts, particularly when using magnetic contacts.

III. Conclusion

In this report, we have demonstrated how different metal contacts with varying Schottky barrier heights can tune the low-temperature transport properties, showing significant differences in electron density and percolative transport behavior. Magnetic contacts could be best suited for exploring and understanding the intrinsic phase transition of 2D semiconductor-based devices. The observed 2D percolation-driven MIT is consistent throughout the temperature range we studied using Co contacts, which provided a low Schottky barrier height compared to the traditional metal contact, such as chromium. Though the intrinsic mechanism could be the same in both types of contacts, the ferromagnetic Co

contact tends to inject a higher carrier density than the Cr contacts. This study will influence the exploration of the intrinsic MIT behavior in low dimensional materials, particularly 2D materials, and paves the way for their implementation into novel quantum devices.

See the supplementary material for the AFM, temperature scaling of Conductivity, Percolation fitting of all temperature.

Conflicts of interest

There are no conflicts to declare.

Acknowledgements

This work was carried out at Jackson State University, Argonne National Laboratory, IL, USA and the National High Magnetic Field Laboratory, FL, USA. Funding was provided by the U.S. Department of Energy, Office of Science, Office of Basic Energy Sciences program under Award Number DE-SC0024072. Use of the Center for Nanoscale Materials, a Department of Energy Office of Science User Facility, was supported by the U.S. DOE, Office of Basic Energy Sciences, under Contract No. DE-AC02-06CH11357. A portion of this work was performed at the National High Magnetic Field Laboratory, which is supported by the National Science Foundation Cooperative Agreements No. DMR-1644779 and DMR-2128556 and the State of Florida.

References

1 P. Wang, M. Hu, H. Wang, Z. Chen, Y. Feng, J. Wang, W. Ling and Y. Huang, Adv. Sci. 2020, 7, 2001116

2 Y. Lee, H. Cho, H. Yoon, H. Kang, H. Yoo, H. Zhou, S. Jeong, G. H. Lee, G. Kim, G. T. Go, J. Seo, T. W. Lee, Y. Hong and Y. Yun*, Adv. Mater. Technol. 2023,* **8***, 2201067*.

3 A. B. Georgescu, P. Ren, A. R. Toland, S. Zhang, K. D. Miller, D. W. Apley, E. A. Olivetti, N. Wagner and J. M. Rondinelli, *Chemistry of Materials*, 2021, **33**, 5591–5605.

4 N. Ali, M. Lee, F. Ali, T. D. Ngo, H. Park, H. Shin and W. J. Yoo, *ACS Appl Mater Interfaces*, 2023, **15**, 13299–13306.

5 S. Zhang and G. Galli, *npj Comput Mater*, 2020, ***6****, 170*.

6 Md. A. Hoque, A. George, V. Ramachandra, E. Najafidehaghani, Z. Gan, R. Mitra, B. Zhao, S. Sahoo, M. Abrahamsson, Q. Liang, J. Wiktor, A. Turchanin, S. Kubatkin, S. Lara-Avila and S. P. Dash, *NPJ 2D Mater Appl*, 2024, **8**, 55.

7 A. Hoffmann, S. Ramanathan, J. Grollier, A. D. Kent, M. J. Rozenberg, I. K. Schuller, O. G. Shpyrko, R. C. Dynes, Y. Fainman, A. Frano, E. E. Fullerton, G. Galli, V. Lomakin, S. P. Ong, A. K. Petford-Long, J. A. Schuller, M. D. Stiles, Y. Takamura and Y. Zhu, *APL Mater. ,2022, **10**, 070904*.

8 Y. J. Lee, Y. Kim, H. Gim, K. Hong and H. W. Jang, *Adv. Mater. 2024, **36**, 2305353*.

9 H. Li, Q. Li, Y. Li, Z. Yang, R. Quhe, X. Sun, Y. Wang, L. Xu, L. Peng, H. Tian, C. Qiu and J. Lu, *Adv Funct Mater*, 2024, **34**, 2402474.

10 E. Abrahams, P. W. Anderson, D. C. Licciardello and T. V Ramakrishnan, *Phys Rev Lett*, 1979, **42**, 673–676.

11 S. Ahn and S. Das Sarma, *Phys. Rev. B, 2022, **105**, 115114*.

12 C. Zhang, S. Kc, Y. Nie, C. Liang, W. G. Vandenberghe, R. C. Longo, Y. Zheng, F. Kong, S. Hong, R. M. Wallace and K. Cho, *ACS Nano*, 2016, **10**, 7370–7375.

13 B. H. Moon, *Emergent Mater*, 2021, **4**, 989–998.

14 Z. Zhao, H. Zhang, H. Yuan, S. Wang, Y. Lin, Q. Zeng, G. Xu, Z. Liu, G. K. Solanki, K. D. Patel, Y. Cui, H. Y. Hwang and W. L. Mao, *Nat Commun, 2015, 6, 7312*.

15 N. R. Pradhan, C. Garcia, B. Chakrabarti, D. Rosenmann, R. Divan, A. V. Sumant, S. Miller, D. Hilton, D. Karaiskaj and S. A. McGill, *Nanoscale*, 2023, **15**, 2667–2673.

16 Y. Liu, N.O. Weiss, X. Duan, H.-C. Cheng, Y. Huang, X. Duan, Van der Waals heterostructures and devices. *Nature Reviews Materials, 2016,* **1**, 16042.

17 R. K. Ghosh and S. Datta, in *2016 International Conference on Simulation of Semiconductor Processes and Devices (SISPAD)*, 2016, pp. 93–96.

18 D. Zhou, Y. Zhou, C. Pu, X. Chen, P. Lu, X. Wang, C. An, Y. Zhou, F. Miao, C. H. Ho, J. Sun, Z. Yang and D. Xing, *npj Quant Mater, 2017,* **2**, 19.

19 N. R. Pradhan, D. Rhodes, Y. Xin, S. Memaran, L. Bhaskaran, M. Siddiq, S. Hill, P. M. Ajayan and L. Balicas, *ACS Nano*, 2014, **8**, 7923–7929.

20 D. Zhang, C. Wen, J. B. Mcclimon, P. Masih Das, Q. Zhang, G. A. Leone, S. V Mandyam, M. Drndić, A. T. C. Johnson Jr. and M.-Q. Zhao, *Adv Electron Mater*, 2021, **7**, 2001219.

21 B. Radisavljevic and A. Kis, *Nat Mater*, 2013, **12**, 815–820.

22 S. Das Sarma, M. P. Lilly, E. H. Hwang, L. N. Pfeiffer, K. W. West and J. L. Reno, *Phys Rev Lett*, 2005, **94**, 136401.

23 S. K. Mallik, R. Padhan, M. C. Sahu, S. Roy, G. K. Pradhan, P. K. Sahoo, S. P. Dash and S. Sahoo, *ACS Appl Mater Interfaces*, 2023, **15**, 36527–36538.

24 V. Podzorov, M. E. Gershenson, C. Kloc, R. Zeis and E. Bucher, *Appl Phys Lett*, 2004, **84**, 3301–3303.

25 N. R. Pradhan, D. Rhodes, Q. Zhang, S. Talapatra, M. Terrones, P. M. Ajayan and L. Balicas, *Appl. Phys. Lett., 2013, 102, 123105*.

26 N. R. Pradhan, Z. Lu, D. Rhodes, D. Smirnov, E. Manousakis and L. Balicas, *Adv. Electron. Mater., 2015, 1: 1500215*.

27 S. K. Mallik, R. Padhan, S. Roy, M. C. Sahu, S. Sahoo and S. Sahoo, *ACS Appl Nano Mater*, 2024, **7**, 4796–4804.

28 S. Fathipour, N. Ma, W. S. Hwang, V. Protasenko, S. Vishwanath, H. G. Xing, H. Xu, D. Jena, J. Appenzeller, A. Seabaugh; *Appl. Phys. Lett.* 10 November 2014, **105** 192101

29 A. Allain, J. Kang, K. Banerjee and A. Kis, *Nature Mater, 2015, **14**, 1195–1205*.

30 X. Cui, E. M. Shih, L. A. Jauregui, S. H. Chae, Y. D. Kim, B. Li, D. Seo, K. Pistunova, J. Yin, J. H. Park, H. J. Choi, Y. H. Lee, K. Watanabe, T. Taniguchi, P. Kim, C. R. Dean and J. C. Hone, *Nano Lett*, 2017, **17**, 4781–4786.

31 A. Dankert, L. Langouche, M. V. Kamalakar and S. P. Dash, *ACS Nano*, 2014, **8**, 476–482.

32 Y. Liu, W. Wu and W. A. Goddard, *J. Am. Chem. Soc.*, 2018, **140**, 550.

33 X. Li, J. T. Mullen, Z. Jin, K. M. Borysenko, M. Buongiorno Nardelli and K. W. Kim, *Phys Rev B*, 2013, **87**, 115418.

34 N. R. Pradhan, A. McCreary, D. Rhodes, Z. Lu, S. Feng, E. Manousakis, D. Smirnov, R. Namburu, M. Dubey, A. R. Hight Walker, H. Terrones, M. Terrones, V. Dobrosavljevic and L. Balicas, *Nano Lett*, 2015, **15**, 8377–8384.

35 L. A. Tracy, E. H. Hwang, K. Eng, G. A. Ten Eyck, E. P. Nordberg, K. Childs, M. S. Carroll, M. P. Lilly and S. Das Sarma, *Phys Rev B*, 2009, **79**, 235307.

36 M. Imada, A. Fujimori and Y. Tokura, *Rev. Mod. Phys., 1998, **70**, 1039*.

37 S. Gupta, F. Rortais, R. Ohshima, Y. Ando, T. Endo, Y. Miyata and M. Shiraishi, *Sci Rep, 2019, **9**, 17032*.

38 N. Kaushik, A. Nipane, F. Basheer, S. Dubey, S. Grover, M. M. Deshmukh and S. Lodha, *Appl. Phys. Lett., 2014, **105**, 113505*.

39 S. Lee, A. Tang, S. Aloni and H. S. Philip Wong, *Nano Lett*, 2016, **16**, 276–281.

40 S. Das, H.-Y. Chen, A. V. Penumatcha and J. Appenzeller, *Nano Lett*, 2013, **13**, 100–105.

41 Mak, K. F.; Shan, J.; Ralph, D. C., *Nature Reviews Physics* **2019,** *1* (11), 646-661.

42 Meng, J.; Lee, C.; Li, Z., *Science Bulletin* **2024,** *69* (9), 1342-1352.

43 W. Wang, Y. Liu, L. Tang, Y. Jin, T. Zhao and F. Xiu, *Sci Rep, 2014, **4**, 6928*.

JACKSON STATE UNIVERSITY
COLLEGE OF SCIENCE, ENGINEERING AND TECHNOLOGY
1400 John R. Lynch Street
Jackson, MS 39217
Dr. Nihar Pradhan
Associate Professor in Physics
Phone: 850-524-0766. FAX: 601-979-3630.
Email: nihar.r.pradhan@jsums.edu
Website: http://www.jsums.edu/physics/nihar-pradhan-ph-d/

Date: 12/02/2024

To
Professor Qing Dai
Associate Editors of the Journal Nanoscale, Royal Society of Chemistry.

Please find below the Data availability Statement

The Data for the submitted article titled "**Percolative phase transition in few-layered $MoSe_2$ Field-effect transistors using Co and Cr contacts"**

The raw data for this article including picture and experimental data of current vs gate voltage, conductivity vs temperature and other data presented in the manuscript are available at request to Dr Nihar R. Pradhan and Dr Stephen A. McGill. The data included in this anuscript included as supplementary information also available in request from the corresponding authors.

Yours sincerely,


Nihar Pradhan Stephen McGill

Dr Nihar Pradhan (Jackson State University, Jackson, Mississippi, USA)
Dr Stephen A McGill (National High Magnetic Field Laboratory, Tallahassee, Florida, USA)